Propagation Characteristics of Symmetric and Asymmetric Multilayer Hybrid Insulator-Metal-Insulator and Metal-Insulator-Metal Plasmonic Waveguides

Mahmoud Talafi Noghani and Mohammad H. Vadjed Samiei*

School of Electrical Engineering, Iran University of Science and Technology, Tehran, Iran
*corresponding author, E-mail: mh_samiei@iust.ac.ir

Abstract

Propagation characteristics of symmetrical and asymmetrical multilayer hybrid insulator-metal-insulator (HIMI) and metal-insulator-metal (HMIM) plasmonic slab waveguides are investigated using the transfer matrix method. Propagation length (L_p) and spatial length (L_s) are used as two figures of merit to qualitate the plasmonic waveguides. Symmetrical structures are shown to be more performant (having higher L_p and lower L_s), nevertheless it is shown that usage of asymmetrical geometry could compensate for the performance degradation in practically realized HIMI waveguides with different substrate materials. It is found that HMIM slab waveguide could support almost long-range subdiffraction plasmonic modes at dimensions lower than the spatial length of the HIMI slab waveguide.

1. Introduction

Plasmonic nanostructures has been considered extensively in recent years as a platform to guide and manipulate plasmonic waves (Surface Plasmon-Polariton (SPP)) at dimensions lower than the diffraction limit. The major challenge in plasmonic waveguides is the metallic loss where it limits the propagation length. Consequently, many designs are proposed to make a balance between confinement and loss based on three primary structures of metal–insulator (MI), insulator–metal–insulator (IMI) and metal–insulator–metal (MIM) [1–8], among which "Hybrid structures" are supposed to be a very promising choice [9]. They have two main advantages: 1. provide better balance between confinement and loss in plasmonic waveguides and 2. provide a very suitable platform for nonlinear devices.

In a hybrid configuration, the dielectric layer next to the metal is decomposed into 3 distinct layers of, low index dielectric (L-layer), high index dielectric (H-layer) and cladding. The main feature of such an arrangement is the efficient coupling of the SPP wave at the metal and L-layer interface with the dielectric wave in the H-layer. The hybrid coupled mode provides a mechanism to control the amount of energy penetration into the metal as well as the spatial extent of wave. Several waveguide configurations (mainly

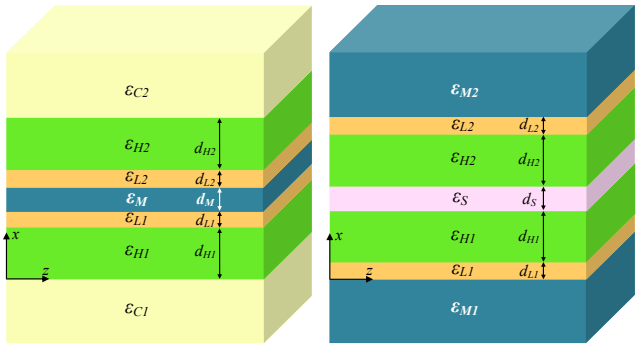

Figure 1: Geometries of hybrid plasmonic slab waveguides: a. hybrid insulator–metal–insulator, and b. hybrid metal–insulator–metal.

2D cross sectional layouts) have already been investigated which may be classified under three groups of HMI, HIMI and HIMI structures, consistent with their non-hybrid counterparts. Analysis of hybrid slab waveguide (HMI type) is performed in refs. [10] and [20]. In refs. [10-14] the 2D constrained HMI waveguide and related devices are investigated. References [15] and [16] deals with 2D HMIM waveguides and [17-19] with 2D HIMI waveguides. Recently, a detailed analysis has been performed on HMI, HIMI and compact form of HMIM slab waveguides so to extract their properties and limits compared to each other and to non-hybrid geometries [21]. The analysis was focused on symmetrical geometries regarding layer thicknesses and dielectric materials.

Here we analyze the symmetrical and asymmetrical HIMI and generalized (non-compact) HMIM slab waveguides (Fig. 1) using the transfer matrix method (TMM) (as discussed in Appendix 1), so to extract and compare their propagation characteristics and their potentials to improve waveguide performances. The "propagation length" and "spatial length" are the two figures of merit (FOM) utilized to qualitate the plasmonic waveguides (Appendix 2). It is shown that the asymmetrical structure provides a mean to compensate for performance degradation caused by realization aspects such as substrate-cladding material difference. When used as a directional coupler (coupled HMI structures from the metal or dielectric side), the

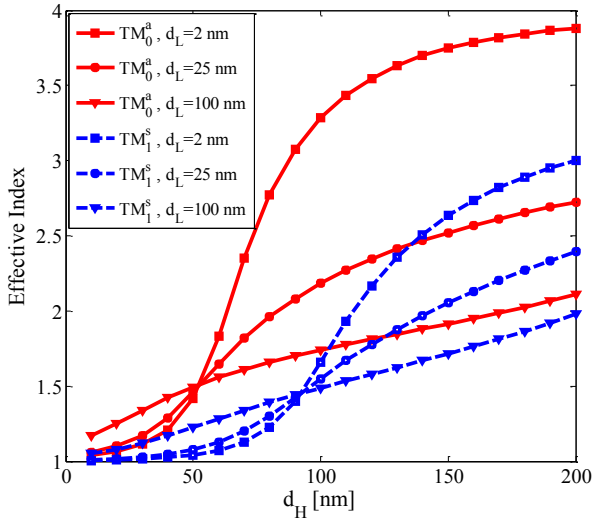

a

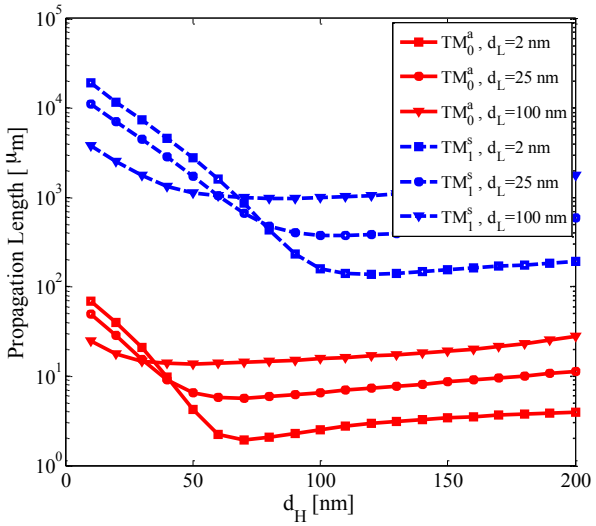

b

Figure 2: a. Effective refractive index and b. Propagation length, of the first two TM polarized hybrid-guided modes of the HIMI slab waveguide in terms of d_H and d_L. Metal thickness is chosen to be d_M=20 nm. Indexes "s" and "a" stand for symmetric and anti-symmetric modes, respectively.

asymmetrical structures presented here could also be used to increase its performance criteria (e.g. extinction ratio).

It is also shown that HMIM waveguide could provide almost long-range propagation at dimensions much lower than ones achieved by the HIMI waveguide, paving a path for realization of long-range subdiffraction SPP waveguides.

2. Symmetrical Structures

Our analysis begins with symmetrical structures where we assume: $\varepsilon_{L1}=\varepsilon_{L2}$, $\varepsilon_{H1}=\varepsilon_{H2}$, $\varepsilon_{C1}=\varepsilon_{C2}$ and $d_{L1}=d_{L2}$, $d_{H1}=d_{H2}$. It is performed at the optical communication wavelength of 1550 nm (193.5 THz). Silica is used for the L and S-layers (spacing layer in HMIM slab waveguide) and silicon is used for the H-layer dielectric material with constants of 2.1 and 12.1, respectively. Cover/cladding layers (ε_C) are assumed to be air. Silver is used for the metal layer due its lower loss

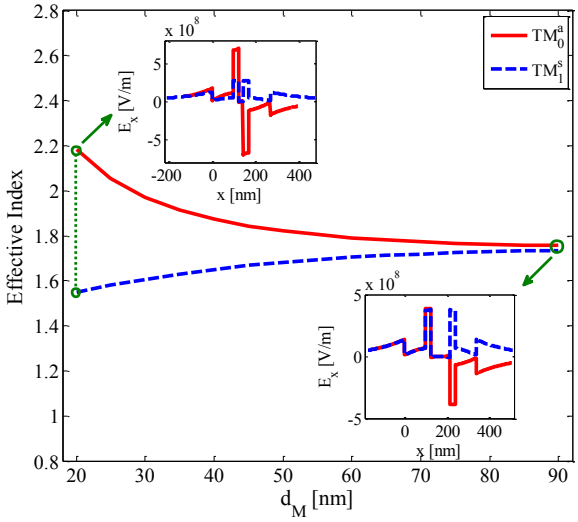

Figure 3: Effective refractive index and Normal electric field (E_x) profile of the first two TM polarized hybrid-guided modes of the HIMI slab waveguide in terms of d_M for d_H=100 nm and d_L=25 nm.

compared to other common metals used in plasmonics. Dielectric function of silver is calculated to be $\varepsilon_{silver}=-127-j3.45$ at λ=1550 nm (by fitting the Drude dielectric function to the measured values of [22,23]).

2.1. Symmetrical HIMI Waveguide

Effective refractive index (Fig. 2(a)) and propagation length (Fig. 2(b)) of the first two TM polarized guided supermodes (asymmetrical short-range TM_0^a and symmetrical long-range TM_1^s) are determined for H-layer thicknesses (d_H) of 10 to 200 nm and L-layer thicknesses (d_L) of 2, 25, and 100 nm. The metal thickness (d_M) is chosen to be 20 nm. The dielectric layer thicknesses are chosen so as to cover a suitable range of values which results in the wide variation of propagation characteristics (effective index and propagation length). Consequently the modal behavior (1st two modes) of the waveguides could be studied directly. The metal layer thickness for the HIMI structure is chosen so as to have a relatively strong coupling between the SPPs on the two side of structure. Extraction of higher order guided modes show that for the aforementioned layer thicknesses, higher supermodes of HIMI waveguide are almost nonpropagative. Variation of effective index due to change in metal thickness from 20 to 90 nm and the normal electric field profile (Ex) at the upper and lower limits are also shown in Fig. 3 in which d_H=100 nm and d_L=25 nm. The metal thickness (dM) in the HIMI slab waveguide controls the coupling strength between the coupled HMI waveguides (HIMI slab waveguide is considered as a coupled waveguide consisting of two similar back-to-back HMI slab waveguides). As d_M decreases, coupling becomes stronger and field profiles of the symmetric and antisymmetric modes depart further from one another. On the other hand, with the increase of d_M, modes become more similar until at about d_M=100 nm they form degenerate modes. It is known that the HIMI waveguide provides subdiffraction long-range propagation via the long-range antisymmetrical TM_1^s mode [21].

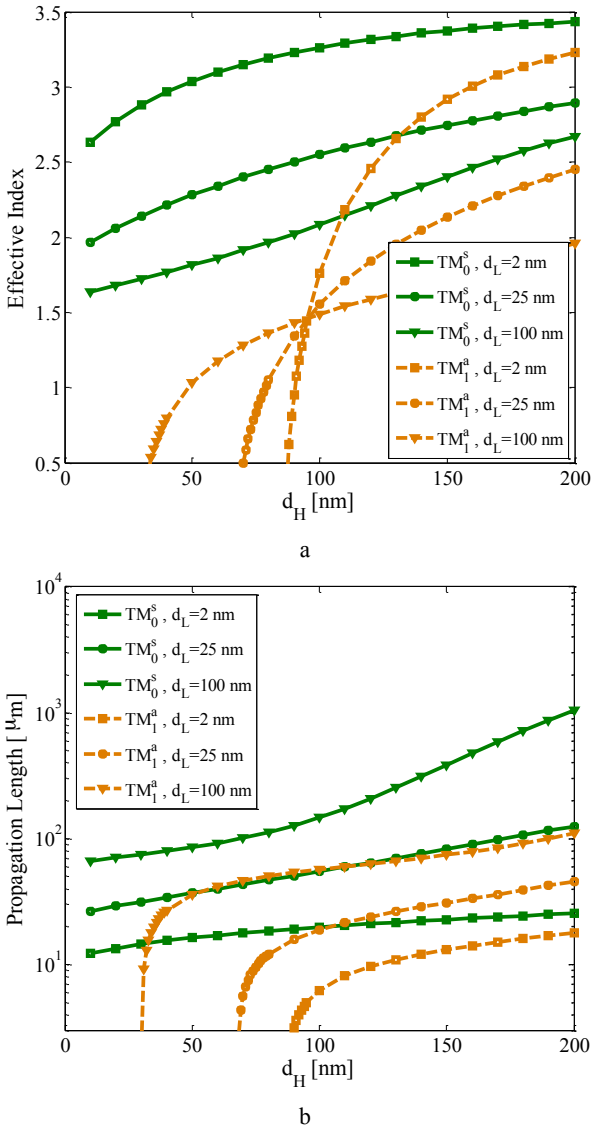

Figure 4: a. Effective refractive index and b. Propagation length, of the first two TM polarized hybrid-guided modes of the HMIM slab waveguide in terms of d_H and d_L. Thickness of the S-Layer is chosen to be d_S=20 nm. Indexes "s" and "a" stand for symmetric and anti-symmetric modes, respectively.

2.2. Symmetrical HMIM Waveguide

Effective refractive index (Fig. 4(a)) and propagation length (Fig. 4(b)) of the first two TM polarized guided modes (symmetrical TM_0^a and antisymmetrical TM_1^s) are determined for d_H=10-200 nm, d_L=2, 25, and 100 nm and d_S=20 nm. Variation of effective index due to change in d_S=20-250 nm and the normal electric field profile (E_x) at the upper and lower limits are also shown in Fig. 5 (with d_H=100 nm and d_L=25 nm).

Similar to the compact HMIM waveguide [21], there is a Quasi-TEM symmetrical mode available in HMIM waveguide (fundamental mode). The second order mode is an antisymmetrical one with a cut-off thickness for d_H (infinite slope for the n_{eff} curves). This means that for d_H smaller than the cut-off thickness, no leaky mode is present

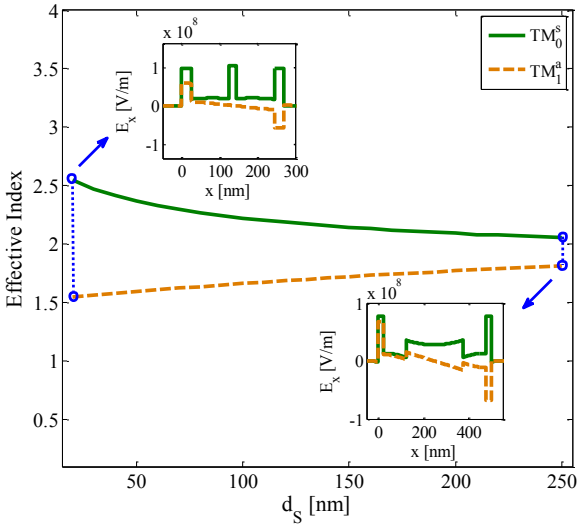

Figure 5: Effective refractive index and Normal electric field (E_x) profile of the first two TM polarized hybrid-guided modes of the HIMI slab waveguide in terms of d_S for d_H=100 nm and d_L=25 nm.

and it becomes guided very rapidly, contrary to the HIMI slab waveguide (Fig. 2(a)) where the modes start as leaky waves with very small slope.

The single mode operation area of the waveguide varies from d_H=0-35 nm for d_L= 100 nm to d_H=0-85 nm for d_L=2 nm. Similar to the HIMI slab waveguide, spacing layer thickness (d_S) controls the coupling strength between the coupled HMI waveguides (with coupling from dielectric side). Decrease/increase in d_S, strengthens/weakens the coupling and consequently the similarize/disimilarize the field profiles of the symmetric and antisymmetric modes. Further discussions are done in the following sections. For d_S larger than 900 nm, the modes become degenerate.

Comparing the propagation length curves of the proposed HMIM slab waveguide (Fig. 4(b)) shows that as the mode order increases, the propagation length decreases. As a result, the fundamental mode (TM_0^a) has the best propagation length. On the other hand, for every mode, propagation length increases by the increase of both d_H and d_L.

3. Asymmetrical Structures

In this section we analyze asymmetrical structures in which asymmetry in dielectric thicknesses is considered. Modes with highest propagation lengths are considered (TM_1^s for HIMI and TM_0^a for HMIM slab waveguides). Waveguides are still assumed to be symmetrical according to dielectric and metallic materials.

3.1. Asymmetrical HIMI Waveguide

Propagation length of HIMI slab waveguide with asymmetry in H-layers are shown in Fig. 6(a). L-layer thicknesses are assumed to be symmetrical with d_L=25 nm. Three cases of d_{H2}=10, 100 and 200 nm for d_{H1}=10-200 nm are considered. In Fig. 6(b), Propagation length of the waveguide with asymmetry in L-layers is plotted. H-layer thicknesses are symmetrical with d_H=10-200 nm. Two cases of (d_{L1}=2 nm ,

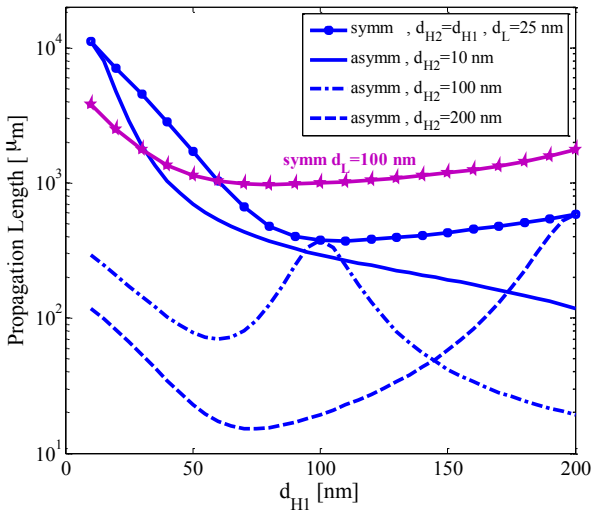

a

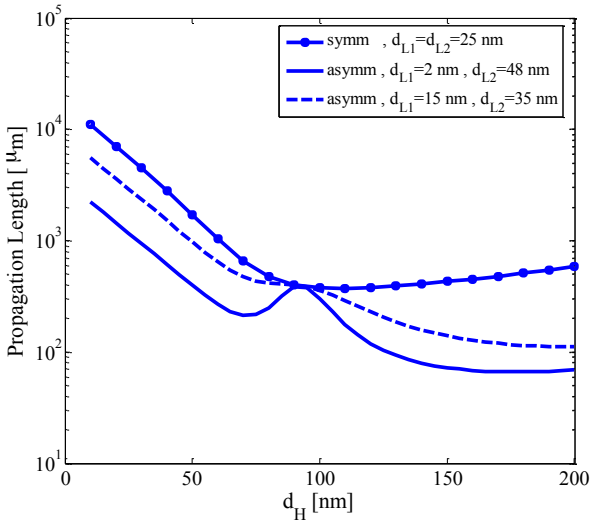

b

Figure 6: Propagation length of the long-range TM_1^s mode of HIMI slab waveguide for: a. asymmetry of the H-Layer thicknesses at $d_{L1}=d_{L2}=d_L$=25 nm (symmetrical cases of d_L=25 and 100 nm are included for comparison), b. asymmetry of the L-Layer thicknesses for $d_{H1}=d_{H2}=d_H$=10-200 nm.

d_{L2}=48 nm) and (d_{L1}=15 nm , d_{L2}=35 nm) are analyzed. The symmetrical case is also shown for comparison.

The plots show that for both groups of asymmetry (H and L-layers), the best propagation length is achieved by the symmetrical geometry. This could be described by the fact that, the HIMI slab waveguide is formed by the coupling of two HMI slab waveguides which results in modes that are complete supermodes (without cut-off thickness (Fig. 2(a))) due to coupling through metal layer (waveguide fields do not interfere with each other very much). According to the coupled mode theory, strongest coupling occurs when the coupled waveguides are fully symmetrical and matching is complete. Therefore, one could conclude from the results obtained here that the minimum loss (maximum propagation length) occurs when the coupling strength reaches its highest value. On the other hand, waveguide loss is proportional to

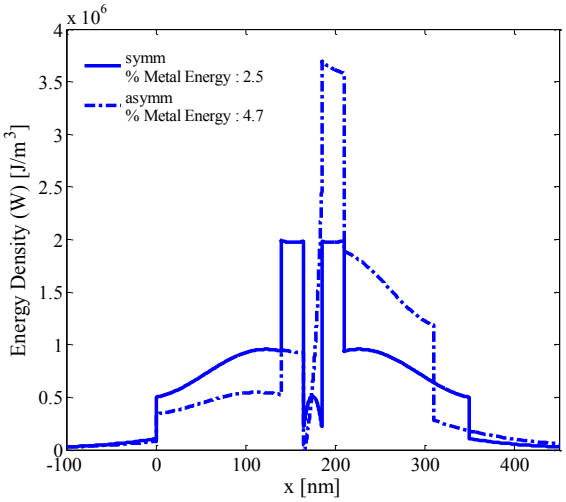

Figure 7: Energy Density of the long-range TM_1^s mode at the cross-section of HIMI slab waveguide with d_L=25 nm, for: 1. symmetrical case with d_H=140 nm, and 2. asymmetrical case with d_{H1}=140 nm and d_{H2}=100 nm. Percentage of energy in metal layer is also included for comparison.

the wave's relative energy density in metal layer. Figure 7 shows the cross-sectional energy density for the two cases of symmetrical (d_H=140 nm) and asymmetrical (d_{H1}=140 nm and d_{H2}=100 nm) waveguides. The increase in energy density of asymmetrical case in metal layer is clearly shown in comparison with the symmetrical one. Calculated relative metal energy (W_n) (normalized to the total energy) is 2.5% for symmetrical and 4.7% for asymmetrical case, consistent with their losses and/or propagation lengths.

A full judgment about the symmetrical and asymmetrical waveguides is accomplished when their transverse confinement ability is calculated using an appropriate quantity. We use the "spatial length" (L_s) as described in appendix 2. Figure 8 displays the results for the same parameters of Fig. 6. One could conclude from the Fig. 8(b) that asymmetry in L-layers decreases the confining ability of waveguide. Figure 8(a) demonstrates that the minimum spatial length is achieved by the symmetrical geometry (L_s=650 nm at d_{H1}=140 nm). Nevertheless, for d_{H1}<90 nm, symmetrical waveguide is more confined although it's propagation length is also shorter. Yet, a different d_L value (other than 25 nm) could be found for which the symmetrical case is superior in both L_s and L_p criteria. For example, symmetrical HIMI slab waveguide with d_L=100 and 25 nm, provides for better performance when d_H<50 nm and d_H>10 nm relative to the asymmetrical cases of (d_{H2}=100, 200 nm) and (d_{H1}=10 nm) respectively. As a concluding remark, a symmetrical geometry of HIMI slab waveguide could always be used to achieve a desired performance.

3.2. Asymmetrical HMIM Waveguide

Propagation length and spatial length of the HMIM slab waveguide considering the asymmetry in H and L-layers are compared with each other and with the symmetrical case in Fig. 9 and 11 respectively. Parameter values are the same as

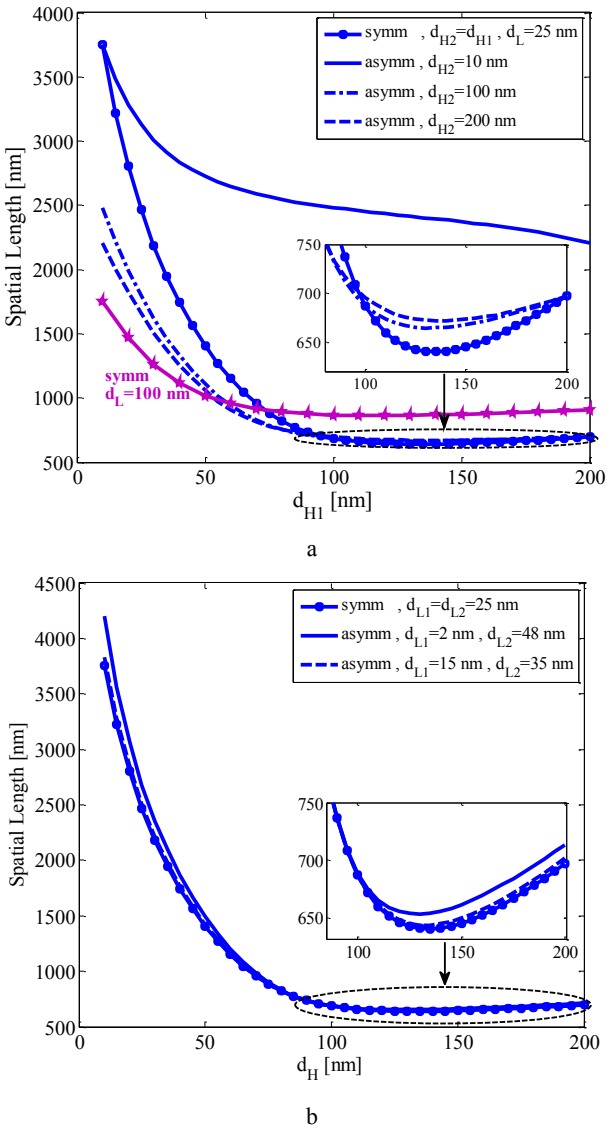

Figure 8: Spatial length of the long-range TM_1^s mode of HIMI slab waveguide for: a. asymmetry of the H-Layer thicknesses at $d_{L1}=d_{L2}=d_L$=25 nm (symmetrical cases of d_L=25 and 100 nm are included for comparison), b. asymmetry of the L-Layer thicknesses for $d_{H1}=d_{H2}=d_H$=10-200 nm.

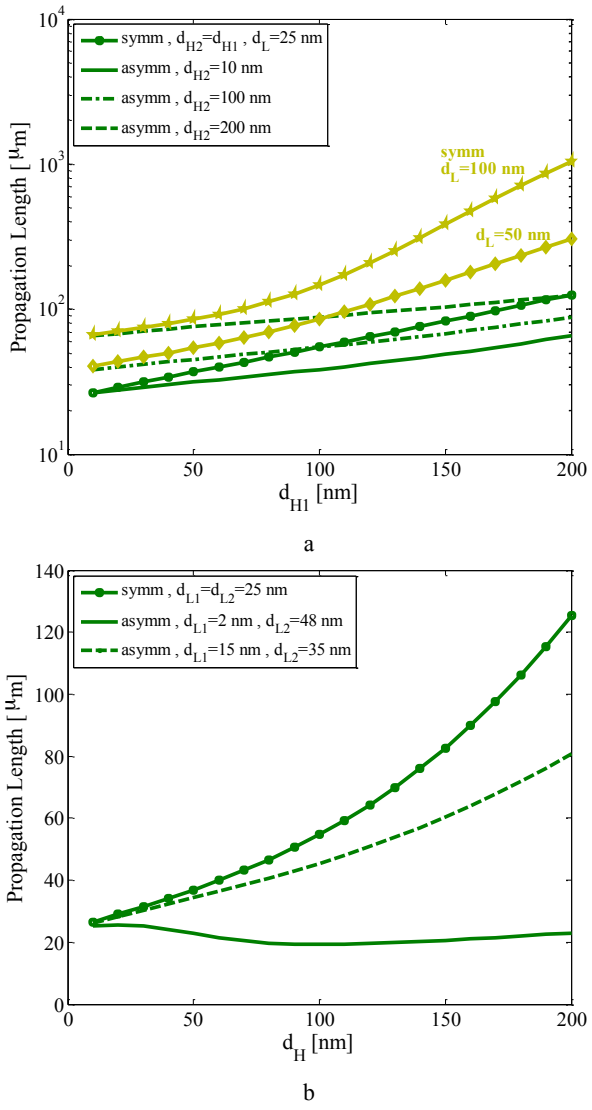

Figure 9: Propagation length of the TM_1^s fundamental mode of HMIM slab waveguide for: a. asymmetry of the H-Layer thicknesses at $d_{L1}=d_{L2}=d_L$=25 nm (symmetrical cases of d_L=25 ,50 and 100 nm are included for comparison), b. asymmetry of the L-Layer thicknesses for $d_{H1}=d_{H2}=d_H$=10-200 nm.

ones used in Fig. 6 and 8. Similar to HIMI waveguide, asymmetry in L-layers increases the loss. But this is not strictly valid for asymmetry in H-layers. In the region where the symmetrical waveguide has longer/shorter propagation length (for 0 <d_{H1}<200 nm when d_{H2}=10 and 200 nm and d_{H1}>100 nm when d_{H2}=100 nm), it also has higher/lower spatial length.

The different behavior of HMIM waveguide from the HIMI waveguide is explained by the fact that, although HMIM waveguide is also composed of two coupled HMI waveguides, but the resulting modes are quite different from the modes of HMI waveguides. This is firstly due to the strong coupling through dielectric layers with strong overlapping fields of each waveguide at the place of the other one, and secondly to the existence of upper and lower metallic layers. Consequently, variation of propagation and spatial lengths with respect to the dielectric layer thicknesses (H and L), is monotone contrary to the HIMI waveguide which have extrema. Since the energy penetration into the metal layer is relatively low, spatial length is almost coincident with the summation of dielectric layer thicknesses. On the other hand, along with the increase in inter-metal separation distance, relative energy density in metal decreases and the propagation length increases (see Fig. 10). Thus, improvement in a criteria results in a degrade in the other. Nevertheless, similar to HIMI waveguide, a different d_L value could be found for which the symmetrical case has a better performance. For example, symmetrical HMIM slab waveguide with d_L=50 nm/100 nm, could perform better relative to the asymmetrical case at d_{H2}=100 nm/200 nm, when d_H<50 nm (see Fig. 9(a) and 11).

3.3. Compensating the Effect of Different Substrate Material

Usage of a suitable substrate material in regards with the choice of fabrication technology, is unavoidable for the

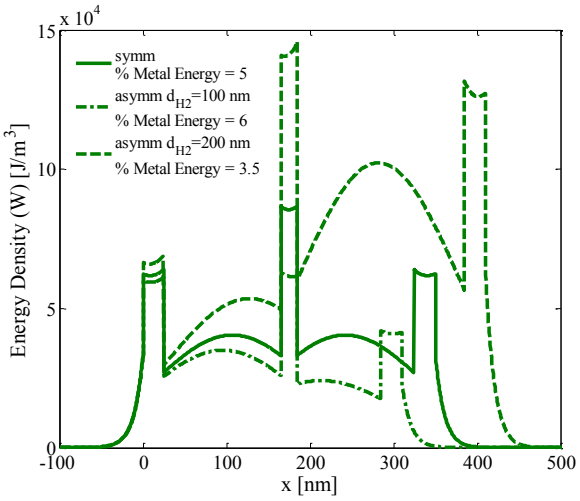

Figure 10: Energy Density of the TM_1^s fundamental mode at the cross-section of HMIM slab waveguide with d_L=25 nm, for: 1. symmetrical case with d_H=140 nm, 2. asymmetrical case with d_{H1}=140 nm and d_{H2}=100 nm, and 3. asymmetrical case with d_{H1}=140 nm and d_{H2}=200 nm. Percentage of energy in metal layer is also included for comparison.

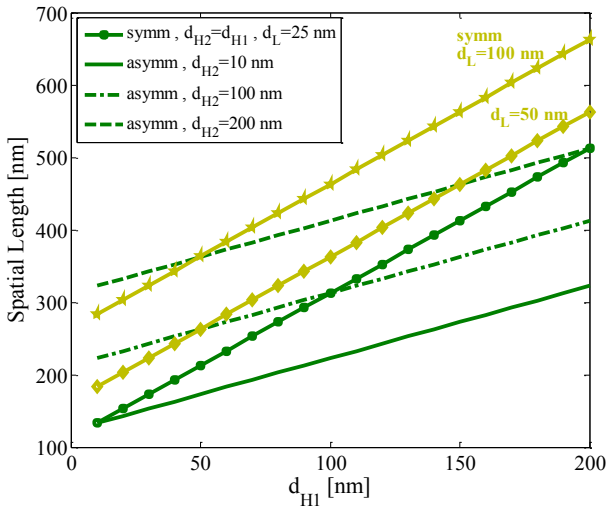

Figure 11: Spatial length of the TM_1^s fundamental mode of HMIM slab waveguide for asymmetry of the H-Layer thicknesses at d_{L1}=d_{L2}= d_L=25 nm (symmetrical cases of d_L=25 ,50 and 100 nm are included for comparison).

realization of aforementioned plasmonic slab waveguides. As a consequence, symmetry of the structures are lost regarding the dielectric materials of the lower and higher layers and thus the waveguide performance is degraded. This isn't a matter of concern in HMIM slab waveguide due to the limited energy penetration into the metal, but it is different in HIMI slab waveguide. Using a silica substrate in HIMI waveguide (ε_{C1}= ε_{Sub}=2.1), not only limits the guided mode region (d_H>~80 nm) (Fig. 12(a)), but also decreases the propagation length (Fig. 12(b)) and increases the spatial length (Fig. 12(c)).

To compensate for this imbalance, we could use asymmetrical dielectric thickness. In fact, an effective index could be considered for each side of the metal. Using a higher index material for the substrate, increases the

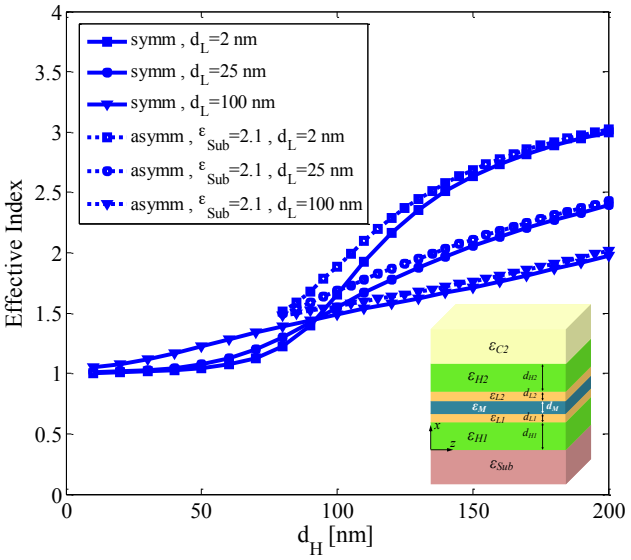

a

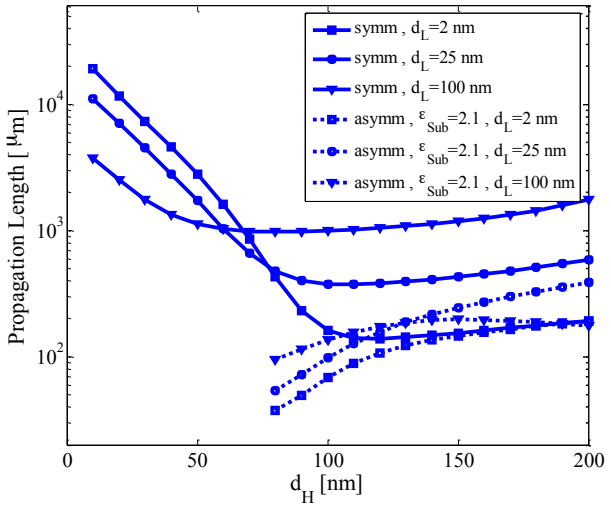

b

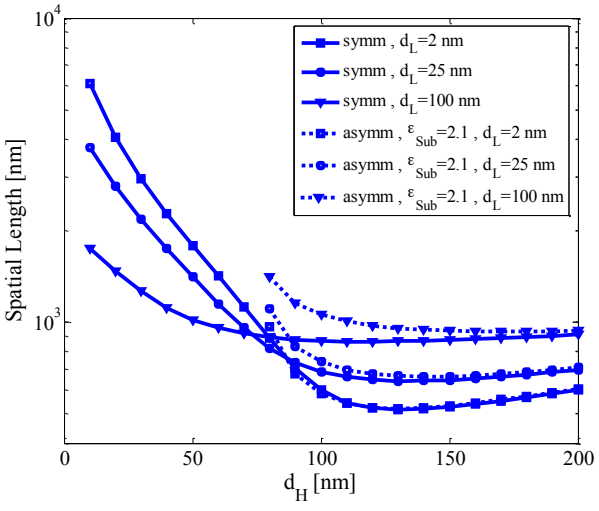

c

Figure 12: Comparing the propagation properties of HIMI slab waveguide with and without silica substrate: a. effective refractive index, b. propagation length and c. spatial length.

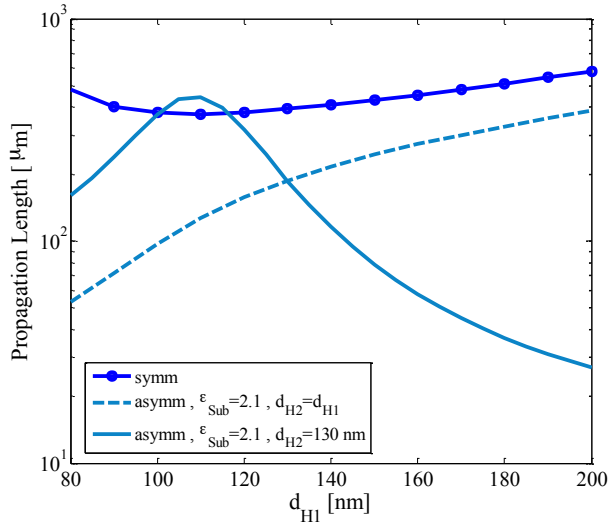

a

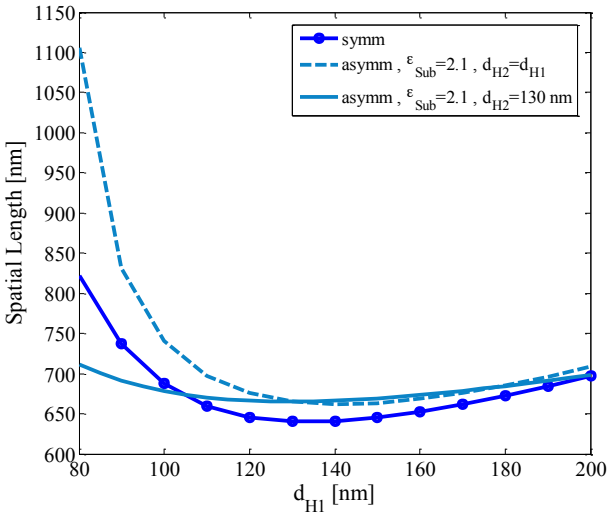

b

Figure 13: Comparing a. the propagation length and b. spatial length of HIMI slab waveguide in three cases of: 1. symmetrical, 2. asymmetrical a with silica substrate and 3. asymmetrical with silica substrate and asymmetry in H-layer thickness (d_{H2}=130 nm).

effective index of the lower side. Balancing the two sides requires either increasing or decreasing the appropriate dielectric layer thicknesses on the upper or lower side respectively (layer thickness corresponds to a weighting coefficient for the index of that layer).

Figure 13 shows the propagation length (Fig. 13(a)) and spatial length (Fig. 13(b)) for three cases: 1. Totally symmetrical, 2. symmetrical thicknesses and asymmetrical material (with silica substrate) and 3. asymmetrical with silica substrate and different H-layer thicknesses. For all cases we have d_L=25 nm. Usage of a H-layer with different thickness (130 nm) improves the propagation length (for d_{H1}=100-115 nm) relative to the maximum propagation length of the case #2, yet keeping the spatial length very low. The performance of symmetrical waveguide is very much retrieved by this method.

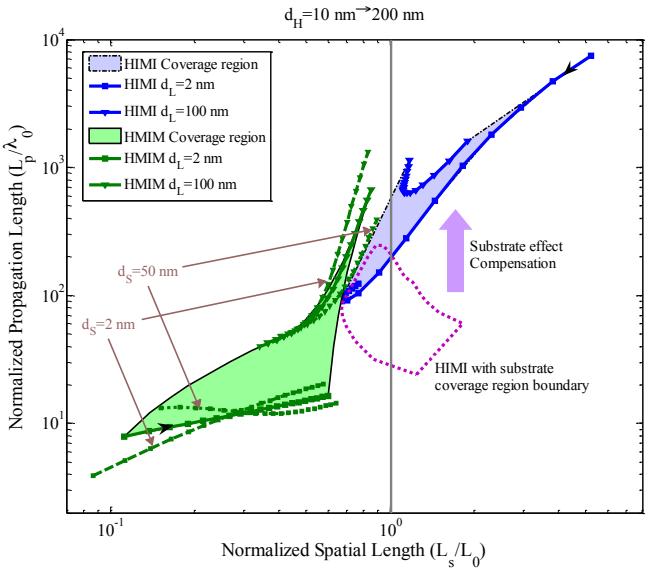

Figure 14: Comparing the HIMI and HMIM slab waveguides using the normalized propagation length (L_p/λ_0) vs. normalized spatial length (L_s/L_0) plot, with: d_M= 20 nm, d_S=2, 20, 50 nm, d_L=2–100 nm, and d_H=10–200 nm. Shaded areas are for d_M= d_S=20 nm.

4. Comparing the Hybrid Waveguides

To finalized the evaluation of HIMI and HMIM slab waveguides, we compare them explicitly through the normalized propagation length (L_p/λ_0) vs. normalized propagation length (L_s/L_0) plot, in which L_0= λ_0/2 is the free space diffraction limit and λ_0 is the free space wavelength. These plots are a suitable form of displaying and comparing the propagation characteristics of plasmonic waveguides, since they are independent of primary parameters (thickness, material, …). Waveguides with the best performance have trajectories toward the top left. This is done in Fig. 14.

The shaded areas show the coverage region of hybrid waveguides regarding the change of d_L from 2 to 100 nm and d_H from 10 to 200 nm for d_M=d_S=20 nm. HMIM waveguide performance variation is also plotted for d_S=2 and 50 nm for two cases of d_L=2 and 100 nm. Free space diffraction limit is shown by a vertical line. The ability of HIMI slab waveguide to propagate long-range mode at dimensions lower than the diffraction limit is clearly shown (contrary to non-hybrid IMI slab waveguide). It is further shown here that the HMIM slab waveguide provides for almost long-range propagation at dimensions lower than the spatial length of HIMI waveguide. This is more obvious for smaller values of d_S (~2 nm). For instance, at normalized propagation length of about 400 (620 μm), normalized spatial length is 1.3 (1000 nm) for HIMI and 0.7 (540 nm) for HMIM slab waveguide. The HMIM waveguide is very much suitable for usage in integrated optics since it provides deep sub-diffraction dimensions as shown in Fig. 14. This is not true for the HIMI structure, since it doesn't cross the diffraction limit line greatly. Instead, HIMI structure provide very long propagation length as well as being more sensitive to dielectric constant variations [21], making it suitable for sensing applications.

5. Conclusions

We have presented a detailed analysis concerning the symmetrical and asymmetrical hybrid insulator-metal-insulator and metal-insulator-metal slab waveguides. Propagation and spatial length is used as two figures of merit to compare the propagation properties of plasmonic waveguides. It is shown that one could always find a symmetrical geometry which is more performant with respect to the asymmetrical case. Nevertheless, asymmetrical waveguide could be used to compensate for performance degradation caused upon using different substrate material for HIMI slab waveguide. It is concluded that the HMIM slab waveguide provides for almost long-range SPP propagation at dimensions lower than the subdiffraction spatial length of HIMI slab waveguide.

Appendix A: Transfer matrix method

The Transfer matrix method is among the most efficient methods for the analysis of multilayer waveguides. Dispersion relation of an arbitrary multilayer structure consisting of homogeneous lossy and lossless layers is formed in a straightforward procedure. The guided mode propagation constants of the waveguide correspond to the zeros of this equation. Here we perform the zero-search using a two step approach. Firstly, an algorithm is used to find the minima of the absolute value of dispersion function *F*. The *F* function for TM-polarized mode (supported by the SPP wave) is defined as follows [24]:

$$F(\gamma) = -j\left(\frac{\gamma_s}{\varepsilon_s} m_{11} + \frac{\gamma_c}{\varepsilon_c} m_{22}\right) - m_{21} + \frac{\gamma_s \gamma_c}{\varepsilon_s \varepsilon_c} m_{12} = 0 \quad \text{(A1)}$$

in which:

$$\gamma_s = \sqrt{\gamma^2 - k_0^2 \varepsilon_s}\ ,\ \gamma_c = \sqrt{\gamma^2 - k_0^2 \varepsilon_c} \quad \text{(A2)}$$

γ is the complex propagation constant ($\gamma = \beta - j\alpha$), ε_s and ε_c are the dielectric constants of substrate and cover layers respectively and m_{ij} coefficients are the total transfer matrix (M_T) elements resulting from the products of M_n ($n=1,...,N$: number of layers) written as:

$$M_T = M_1 M_2 ... M_N = \begin{bmatrix} m_{11} & m_{12} \\ m_{21} & m_{22} \end{bmatrix},$$
$$M_n = \begin{bmatrix} \cos(k_n d_n) & -\frac{j\varepsilon_n}{k_n}\sin(k_n d_n) \\ -\frac{jk_n}{\varepsilon_n}\sin(k_n d_n) & \cos(k_n d_n) \end{bmatrix} \quad \text{(A3)}$$

where

$$k_n = \sqrt{k_0^2 \varepsilon_n - \gamma^2} \quad \text{(A4)}$$

and ε_n, d_n are the layer n dielectric constant and thickness respectively.

The number of minima of $|F|$ function equals to the number of propagating modes (M). The minima of $|F|$ could be verified using real part of complex propagation constant (β:phase constant), since β is greater than α (attenuation constant), by some orders of magnitude. Once β_{min} are found, they could be used as initial values for a suitable zero finding code to find $\gamma_m = \beta_m - j\alpha_m$ ($m=1,...,M$). Using γ for each mode, the tangential electromagnetic fields at every point within layer n could be expressed as a function of fields at the bottom of that layer as:

$$\begin{bmatrix} H_{y_n}(x) \\ \omega\varepsilon_0\varepsilon_n E_{z_n}(x) \end{bmatrix} = \begin{bmatrix} -\cos[k_n(x - x_n)] & -\frac{j}{k_n}\sin[k_n(x - x_n)] \\ -jk_n \sin[k_n(x - x_n)] & \cos[k_n(x - x_n)] \end{bmatrix}^{-1} \cdot \begin{bmatrix} H_{y_{n-1}}(x_n) \\ \omega\varepsilon_0\varepsilon_n E_{z_{n-1}}(x_n) \end{bmatrix} \quad \text{(A5)}$$

where x_n is the lower boundary coordinate of the n'th layer.

Appendix B: Figures of merit

Among the different figures of merit used to quantify the trade-off between confinement and loss in plasmonic waveguides we have used: propagation length (L_p) and spatial length (L_s). Propagation length is the distance wherein the electric field intensity of a wave decays by a factor of 1/e, defined by:

$$L_p = \frac{1}{2|\mathrm{Im}(\gamma)|} = \frac{1}{2\alpha} \quad \text{(B1)}$$

Spatial length, describes the spatial extent of the propagating mode by the distance between the points in the cladding and substrate regions where the electric field decays to 1/e of its peak value. Spatial length, in another words, is the physical length of the propagating mode and is a descriptor representing the integration ability of a plasmonic waveguide and is written as:

$$L_s = \sum_{n=1}^{N}\left[d_n + \mathrm{Re}\left(\frac{1}{\gamma_s}\right) + \mathrm{Re}\left(\frac{1}{\gamma_c}\right)\right] \quad \text{(B2)}$$

References

[1] P. Berini, "Plasmon-polariton waves guided by thin lossy metal films of finite width: Bound modes of symmetric structures," *Phys. Rev. B*, vol. 61, no. 15, pp. 10484-10503, Nov. 2000.

[2] R. Zia, M.D. Selker, and M.L. Brongersma, "Leaky and bound modes of surface plasmon waveguides," *Phys. Rev. B*, vol. 71, no.16, pp. 165431, Apr. 2005.

[3] R. Zia, M.D. Selker, P.B. Catrysse, and M.I. Brongersma, "Geometries and materials for subwavelength surface plasmon modes," *J. Opt. Soc. Am. A*, vol. 21, no. 12, pp. 2442-2446, Dec. 2004.

[4] G. Veronis, and S. Fan, "Guided subwavelength plasmonic mode supported by a slot in a thin metal film," *Opt. Lett.*, vol. 30, no. 24, pp. 3359–3361, Dec. 2005.

[5] I. Breukelaar, R. Charbonneau and P. Berinim, "Long-range surface plasmon-polariton mode cutoff and radiation," *Appl. Phys. Lett.,* vol. 88, no. 5, pp. 051119, Feb. 2006.

[6] S. I. Bozhevolnyi, V. S. Volkov, E. Devaux, J. Y. Laluet and T. W. Ebbesen, "Channeling surface plasmons," *Appl. Phys. A,* vol. 89, no. 2, pp. 225-231. Nov. 2007.

[7] T. Holmgaard and S. I. Bozhevolnyi, "Theoretical analysis of dielectric-loaded surface plasmon-polariton waveguides," *Phys. Rev. B,* vol. 75, pp. 1-12. June 2007.

[8] A. V. Krasavin and A. V. Zayats, "Passive photonic elements based on dielectric-loaded surface plasmon polariton waveguides," *Appl. Phys. Lett.*, vol. 90, no. 21, pp. 211101, May 2007.

[9] R. F. Oulton, V. J. Sorger, D. A. Genov, D. F. P. Pile, and X. Zhang, "A hybrid plasmonic waveguide for subwavelength confinement and long-range propagation," *Nature Photonics*, vol. 2, no. 8, pp. 496-500, Jul. 2008.

[10] R. Salvador, A. Martinez, C. G. Meca, R. Ortuno and J. Marti, "Analysis of Hybrid Dielectric Plasmonic Waveguides," *IEEE J. of Selec. Topics in Quantum Elec.*, vol. 14, no. 6, pp. 1496-1501. Nov. 2008.

[11] M. Fujii, J. Leuthold and W. Freude, "Dispersion relation and loss of subwavelength confined mode of metal-dielectric-gap optical waveguides," *IEEE Photonics Tech. Lett.*, vol. 21, no. 6, pp. 362–364. March 2009.

[12] D. Dai and S. He, "A silicon-based hybrid plasmonic waveguide with a metal cap for a nano-scale light confinement," *Optics express*, vol. 17, no. 19, pp. 16646-53. Sep. 2009.

[13] H. S. Chu, E. P. Li, P. Bai and R. Hegde, "Optical performance of single-mode hybrid dielectric-loaded plasmonic waveguide-based components," *Appl. Phys. Lett.*, vol. 96, no. 2, pp. 1-3, June 2010.

[14] H. S. Chu, P. Bai, E. P. Li and W. R. J. Hoefer, "Hybrid Dielectric-Loaded Plasmonic Waveguide-Based Power Splitter and Ring Resonator: Compact Size and High Optical Performance for Nanophotonic Circuits," *Springer Plasmonics,* vol. 6, no. 3, pp. 591-597, Sep. 2011.

[15] D. Dai and S. He, "Low-loss hybrid plasmonic waveguide with double low-index nano-slots," *Optics Express*, vol. 18, no. 17, pp. 2133-2135. Aug. 2010.

[16] J. T. Kim, "CMOS-Compatible Hybrid Plasmonic Waveguide for Subwavelength Light Confinement and On-Chip Integration," *IEEE Photonics Tech. Lett.*, vol. 23, no. 4, pp. 206-208, Feb. 2011.

[17] Y. Bian, Z. Zheng, X. Zhao, J. Zhu and T. Zhou, "Symmetric hybrid surface plasmon polariton waveguides for 3D photonic integration," *Optics express*, vol. 17, no. 23, pp. 21320-5, Nov. 2009.

[18] J. T. Kim, J. J. Ju, S. Park, M. S. Kim and S. K. Park, "Hybrid plasmonic waveguide for low-loss lightwave guiding," *Optics express*, vol. 18, no. 13, pp. 2808-2813, Feb. 2010.

[19] Y. Kou, F. Ye and X. Chen, "Low-loss hybrid plasmonic waveguide for compact and high-efficient photonic integration," *Optics express*, vol. 19, no. 12, pp. 11746-52, June 2011.

[20] M. Z. F. Alam, J. S. Aitchison and M. Mojahedi, "Theoretical Analysis of Hybrid Plasmonic Waveguide," *IEEE J. of Selected Topics in Quantum Electronics,* vol.19, no.3, pp.4602008, May-June 2013.

[21] M. T. Noghani and M. H. V. Samiei, "Analysis and Optimum Design of Hybrid Plasmonic Slab Waveguides," *Springer Plasmonics*, vol. 8, no. 2, pp. 1155-1168, June 2013.

[22] P. B. Johnson and R. W. Christy, "Optical Constants of the Noble Metals," *Phys. Rev. B* , vol. 6, no. 12, pp. 4370-4379, Dec. 1972.

[23] M. J. Weber, *Handbook of Optical Materials* , CRC Press, Boca Raton, Florida, US, 2003.

[24] E. Anemogiannis and N. E. Glytsis, "Multilayer Waveguides: Efficient Numerical Analysis of General Structures," *IEEE J. of Lightwave Tech.*, vol. 10, no. 10, pp. 1344-1351, Oct. 1992.